Modeling the effect of the structure of polymer photocells on their absorption spectrum

Rafi Shikler[a] and Richard H. Friend
Cavendish Laboratory - J. J. Thomson Avenue, Cambridge CB3 0HE, United Kingdom

(Received 10 December 2006; accepted 28 May 2007; published online 9 July 2007)

We present a framework for the calculation of light absorption in multicomponent polymer photocells. We have modeled a periodic lateral structure of two polyfluorene conjugated polymers with complementary absorption spectra. We show how the coupling induced by scattering at the interfaces between different regions of the structure leads to enhanced absorption arising from energy flow from the less-absorbing to the more-absorbing material. We also show that a periodic structure can lead to resonance amplification of absorption in part of the absorption spectrum. These lead to an enhancement in the numerically calculated absorption spectrum by up to 2.6 times. We further show that a periodic lateral structure can show larger optical absorption than similar devices with a bilayer structure. This method is generally applicable to multicomponent heterojunction photovoltaic diodes. © *2007 American Institute of Physics*. [DOI: 10.1063/1.2752547]

I. INTRODUCTION

Organic polymer solar cells[1–3] open the possibility of fabricating inexpensive large-area devices that can be flexible and could be processed into complex shapes, thus leading to innovative photovoltaic applications.[4] Charge generation in these devices requires the presence of heterojunctions formed between electron- and hole-accepting materials to ionize the excitons formed by optical absorption. Direct mixing in solution of both components with controlled demixing on solvent evaporation following film deposition has been widely investigated, and cells made from blends of hole-accepting poly(hexylthiophene) and electron-accepting fullerenes show efficiencies as high as 5%,[5] but further improvements are needed for this technology. Understanding the role played by the morphology/structure of these devices in determining their overall performance can lead to more efficient devices based on improved architecture. Various researches studied the effect of polymer blend morphology on device performance.[6,7] The experimental approach can gain much by supplementing it with computational techniques. The computational studies can guide choices regarding device architectures for improved solar cell performance.

The first process in harvesting the sunlight is the absorption of light. It usually enters into any device simulation via a generation term. The absorption in solar cell devices is usually treated only in one dimension. The absorption profile used in these calculations either has the form of an exponential decay[8] or is solved using the transfer matrix method.[9–11] Recent simulation by Walker *et al.*,[12] who simulated phase separation in polymer blends, and Buxton *et al.*,[8] who simulated diblock copolymer, used the above techniques. These approaches neglect the effect of scattering, which is correct when the typical length scale of lateral features is much smaller than the wavelength of the incident light. However, this need not be the case in real devices. In order to understand the effect of device structure on its absorption spectrum, it is important to calculate the correct absorption profile using numerical methods that take into account the process of scattering.

The aim of this work is to develop a framework that will enable researchers to calculate the absorption profile for arbitrary structures. The framework is based on an implementation of Yee's algorithm, finite difference time domain (FDTD),[13,14] to solve Maxwell's equations.

II. EXPERIMENT

In this work we have calculated the absorption of a polymer photocell made of two polyfluorene-based polymers: poly(9,9′-dioctylfluorene-co-bis-*N*,*N*′-(4- butylphenyl)-bis-*N*,*N*′-phenyl-1,4-phenylene-diamine) [PFB] as the high-mobility hole transporting polymer[15] and poly(9,9′-dioctylfluorene-co-benzo-thiadiazole) [F8BT] as a high-mobility electron transport. Their absorption spectra can be seen in Fig. 1.

These materials were chosen because the dependence of the refraction index, n, and the extinction coefficient, k, on the wavelength of the electromagnetic field (EM) is available for both materials,[16] and because their absorption spectra

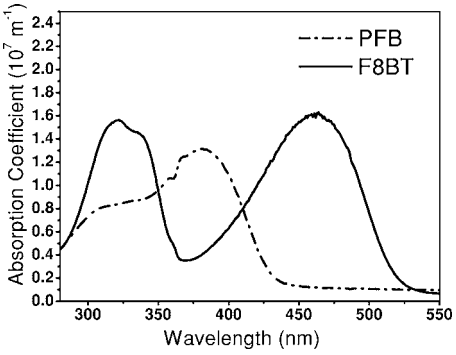

FIG. 1. The dependence of the absorption coefficient of PFB (dash-dot line) and F8BT (solid line) on wavelength (Ref. 17).

[a]Electronic mail: rafi.shikler@gmail.com

 © 2007 American Institute of Physics

Downloaded 05 May 2010 to 132.72.54.88. Redistribution subject to AIP license or copyright; see http://jap.aip.org/jap/copyright.jsp

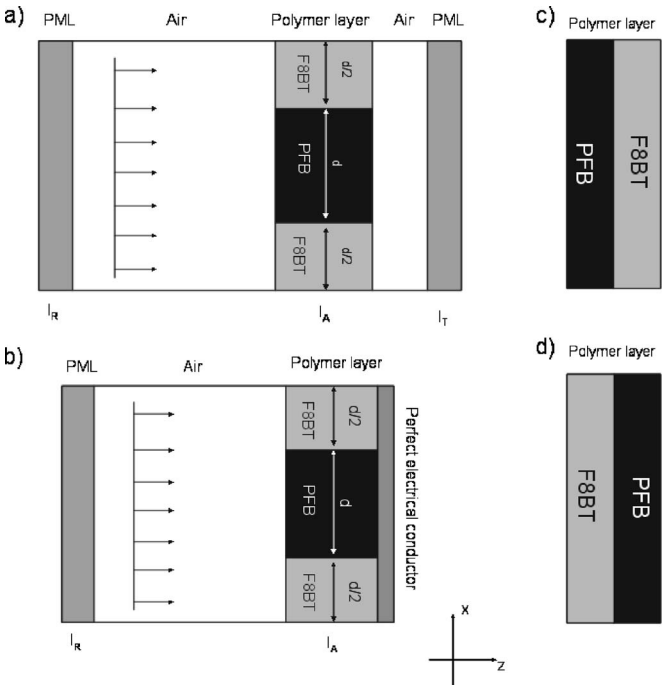

FIG. 2. The different types of architectures used in this research. Both domain types lay in the x-z plane and are infinite in the y direction. The difference between the first two structures is the presence (b) or absence (a) of mirror at the end of the polymer layer. (c) and (d) show the two possible bilayer structures for the polymer. A detailed description of these structures is given in the text.

complement each other. Our approach can be applied to any two materials. In this research we have used different types of structures for the photoactive organic layers.

Figure 2(a) shows one of the structure types used in this research. The layered structure is built of (from left to right):

(1) A perfectly matched layer (PML)—This layer is used to calculate the intensity of the reflected waves from the polymer layer (the third layer), I_R, and to simulate an artificial extension to infinity of the device. At the beginning of this layer, at $z=0$, there is a mirror made from a perfect electric conductor (PEC).
(2) Air—This layer incorporated a plane-wave source. The plane wave has TE_y polarization and is propagating in the positive z direction.
(3) Polymer layer–This layer serves as the active layer of the device. The width of the layer, i.e., the period of the structure, is $2d$. This is the control parameter of the structure. The discretized Maxwell's equations have periodic boundary conditions in the x direction due to the device structure. The absorbed intensity, I_A, is calculated for this layer.
(4) Air—This layer simulates the interface between the active layer and the outer world.
(5) PML–This layer is used to calculate the intensity of the transmitted wave, I_T. It also serves as an artificial layer that simulates a device which is extended to infinity in the positive z direction. At the end of the layer there is a PEC that serves as a mirror.

Figure 2(b) shows an alternative configuration that is used in thin-film organic solar cells. In this configuration, the fourth and fifth layers are replaced by a mirror made of a PEC. This results in a device that has only four and not five layers. Figures 2(c) and 2(d) show alternative configurations that are used for polymer photocells and were used in this study. They are called bilayer and were studied both in a mirror and a mirrorless configuration.

As can be seen in Fig. 2, we have chosen to conduct the calculations on structures that are constructed from pure regions of F8BT and PFB. This is achievable in bilayer structures but is yet to be achieved in lateral structures. It is important to study these structures in order to check if the effort invested in creating pure domains is justified or whether a better structure can be found.

The PML layers are designed and implemented using the Berenger method.[18] The plane wave was generated using the total-field/scatter-field (TF/SF) formulation.[14,19–21] The propagation and absorption of EM waves are governed by the Maxwell equations. The equations that describe the propagation of a TE_y wave are

$$\frac{\partial E_x}{\partial t} = -\frac{1}{\epsilon}\left[\frac{\partial H_y}{\partial z} - (\sigma E_x)\right], \tag{1}$$

$$\frac{\partial E_z}{\partial t} = \frac{1}{\epsilon}\left[\frac{\partial H_y}{\partial x} - (\sigma E_z)\right], \tag{2}$$

$$\frac{\partial H_y}{\partial t} = \frac{1}{\mu}\left[\frac{\partial E_z}{\partial x} - \frac{\partial E_x}{\partial z} - (\sigma^* H_y)\right], \tag{3}$$

where E_x, E_z, H_y are the relevant components of the electromagnetic field. ϵ and μ are the real parts of the electric permittivity and magnetic permeability, σ and σ^* are the electric conductivity and equivalent magnetic loss, respectively. The last two parameters can also be written as $\sigma/\sigma^* = \omega \times \mathrm{Im}(\epsilon/\mu)$, where ω is the frequency of the electromagnetic wave. The absorbance in energy per unit volume per unit time is calculated using the following formula:

$$Q = \frac{1}{T}\int_{t_0}^{t_0+T} \mathrm{Im}(\epsilon)\omega|\mathbf{E}|^2 + \mathrm{Im}(\mu)\omega|\mathbf{H}|^2 \mathrm{d}t$$
$$= \frac{1}{T}\int_{t_0}^{t_0+T} \sigma|\mathbf{E}|^2 + \sigma^*|\mathbf{H}|^2 \mathrm{d}t, \tag{4}$$

where T is the period of the EM wave. The initial time t_0 was chosen as a time much larger than the time it takes the EM wave to travel the distance between the plane-wave source and the end of the device. This was found by plotting $|E(t+T,\mathbf{r})|/|E(t,\mathbf{r})|$ for both E_x and E_z with $\mathbf{r}$ inside the active polymer layer. We then chose t_0 to be in the region where this ratio is equal to 1.

In this time region we have calculated the following quantities:

Downloaded 05 May 2010 to 132.72.54.88. Redistribution subject to AIP license or copyright; see http://jap.aip.org/jap/copyright.jsp

$$I_R \equiv \int_{\text{left PML}} Q\, dx\, dz,$$

$$I_{\text{abs}} \equiv \int_{\text{polymer layer}} Q\, dx\, dz,$$

$$I_T \equiv \int_{\text{right PML}} Q\, dx\, dz. \quad (5)$$

The first two quantities, I_R, I_{abs}, the reflective and absorbed intensities, respectively, were calculated for both configurations. The last quantity, I_T, the transmitted intensity, exists only in the first configuration. The total intensity scales quadratically with the device cross section, i.e., the period of the polymer structure, $2d$. Therefore, we have to normalize it to enable comparison between different devices. The best way to do it is to divide the reflected, absorbed, and transmitted (if existing) intensities by the total intensity $I=I_T+I_{\text{abs}}+I_R$ or $I=I_{\text{abs}}+I_R$ for the first and second configurations, respectively. The new quantities depicted the percentage of the total intensity that is reflected, absorbed, or transmitted.

We start by comparing the predictions for the dependence of the absorption on the structure's period of the no-scattering approach and numerical calculations including scattering as shown in Figs. 2(a) and 2(b). In order to compare our numerical calculation with the nonscattering approach, the normalized values were further divided by the corresponding values for the case where the effect of the interfaces is neglected, i.e., no scattering by the structure,

$$\hat{I}_{\text{abs}} = \frac{I_{\text{numerical}}}{I_{\text{no-scattering}}}. \quad (6)$$

If $\hat{I}_{\text{abs}}$ is larger than 1, it means that the no-scattering approach underestimates the absorption while it overestimates for $\hat{I}_{\text{abs}}$ smaller than 1. $I_{\text{no-scattering}}$ is independent of the structure period and therefore $\hat{I}_{\text{abs}}$ can also be used to compare the efficiency of absorption for different structures' periods. The dependence of this quantity on the excitation wavelength and structure period, $2d$, is summarized in Fig. 3.

Figure 3 can be divided into at least four different areas:

(1) Excitation wavelengths below 350 nm for all structure periods. In these areas the absorption ratio is very close to 1; hence, the no-scattering and numerical calculations are equal. An additional result is that the absorption is structure independent in this region.
(2) Excitation wavelength between 350 and 380 nm with variable sizes in the structure period domain. In these areas the calculation that neglects scattering underestimates the absorption by up to a factor of 1.3.
(3) Excitation wavelengths centered around 450 nm whose dependence on the structure period decreases with the increase in film thickness. These areas have the largest value $\hat{I}_{\text{abs}}$ and hence the largest underestimation of the absorption by the nonscattering method by up to 2.6 times, as can be seen in Fig. 3(f).
(4) Two lobes in the long wavelength region (above 450 nm) that roughly have the linear dependence of excitation wavelength on the structure period. The linear coefficients are $\simeq 1$, 2. The absorption in these areas strongly depends on the film thickness and the presence or absence of a mirror at the end of the polymer layer.

We have also compared devices having lateral period and the bilayer structures depicted in Figs. 2(c) and 2(d). The results are summarized in Fig. 4. The quantity plotted in this figure as function of excitation wavelength and structure period is

$$\hat{I} = \frac{I_{\text{periodic}}}{I_{\text{bilayer(PF/FP)}}},$$

where I_{periodic} is the same as $I_{\text{numerical}}$ before and I_{bilayer} is the calculated absorption for a bilayer structure. The subscripts "PF" and "FP" signify the order of the layers F8BT on top of PFB and PFB on top of F8BT, respectively. The thickness of both the lateral periodic structure and the bilayer structure is 50 nm.

The following observation can be deduced from Fig. 4:

- Figures 4(a) and 4(b) have enhancement of absorption around excitation wavelength that corresponds to a minimum in the absorption coefficient of the F8BT around 350–375 nm. Both have enhancement lobes where there is a linear dependence of excitation wavelength on the structure period.
- In Fig. 4(c) the effect of the mirror changes the enhancement to the regions corresponding to the minima of PFB or the maxima of F8BT around 330 and 440 nm. In Fig. 4(d) the dominant effect is the enhancement at the lobes where there is a linear dependence of excitation wavelength on the structure period. This effect is so pronounced that it dominates the entire spectrum.
- It can be seen that in large part of absorption spectrum, the lateral periodic structure absorbs more light than the two bilayer structures. This is especially true for the PF configuration, which is the one mostly used in devices.

III. DISCUSSION

In this section we explain the observed behavior in Fig. 3 for the samples without the presence of a mirror and indicate how our reasoning can be applied to the structures with a mirror. We then draw upon our conclusions and explain the observations in Fig. 4. These observation led us to deduce new design rules for future devices.

The first step is to study the absorption coefficient of the individual homopolymers. The dependence of the absorption coefficient on wavelength for F8BT and PFB is shown in Fig. 1

By studying the dependence of the absorption coefficient on the wavelength and comparing it to the results depicted in Figs. 3(a), 3(c), and 3(e), we can see that the first region, the region with excitation wavelength smaller than 350 nm, is a region where both F8BT and PFB have large absorption coefficients. In this region we can expect that the interface

Downloaded 05 May 2010 to 132.72.54.88. Redistribution subject to AIP license or copyright; see http://jap.aip.org/jap/copyright.jsp

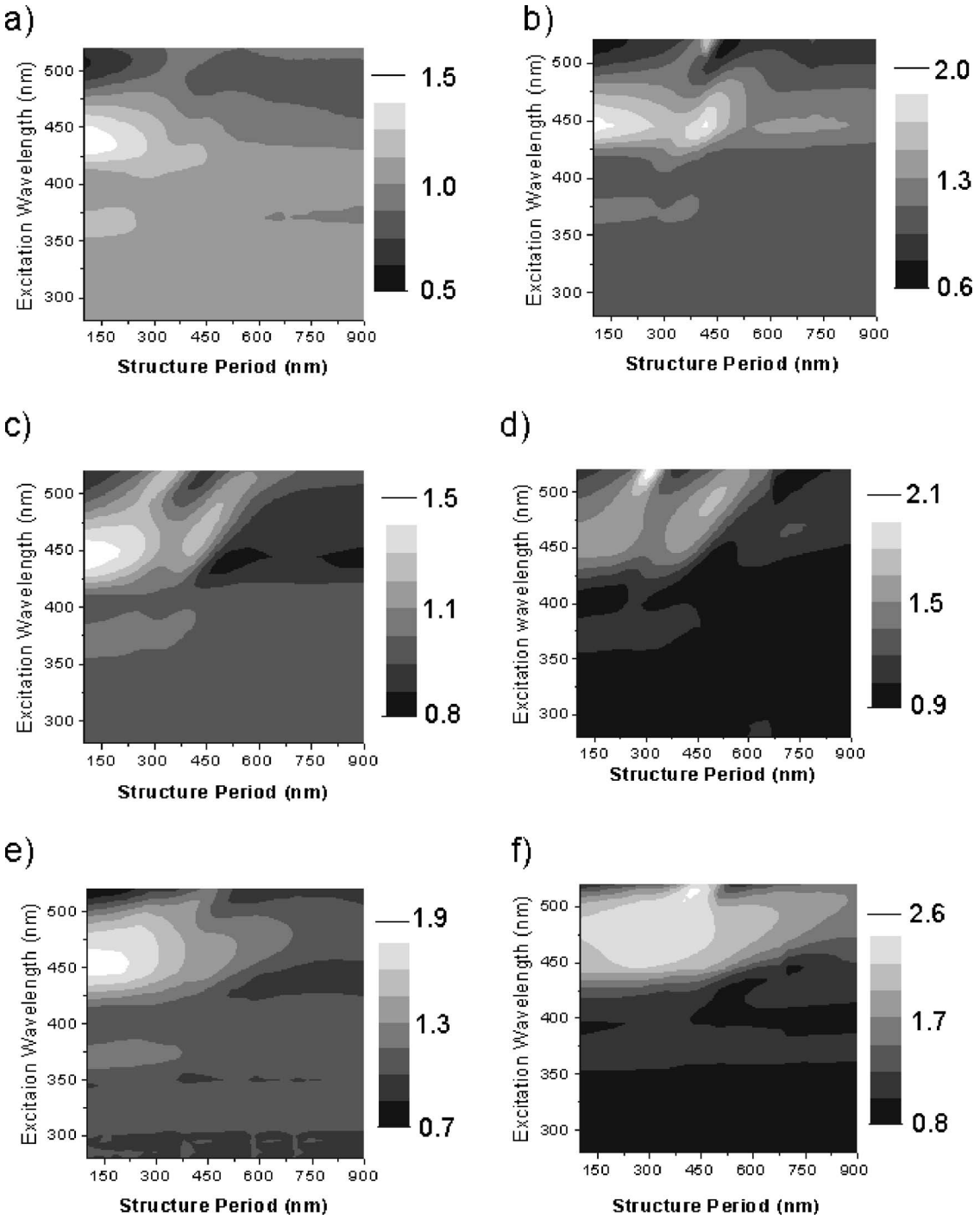

FIG. 3. The dependence of $\hat{I}_{abs}$ on the structure period, $2d$, and on the excitation wavelength for different film thicknesses and different device structures. Film thickness 50 nm (a) and (b), 100 nm (c) and (d), and 200 nm (e) and (f). (a), (c), and (e) are without a mirror while (b), (d), and (f) are with a mirror at the end of the device. Enhanced absorption is indicated by brighter colors, with values of $\hat{I}_{abs}$ as indicated by the corresponding bars.

between the PFB and F8BT will have little or no effect on the propagating wave front. As can be seen in Fig. 3, this is indeed the case.

The second and third regions in Fig. 3 are the regions where the absorption coefficients of either F8BT or PFB have a minimum. To understand the observed increase in the absorption ratio we have calculated the Poynting vector, S, at excitation wavelength of 360 and 440 nm for structure having period of 180 nm and film thickness of 1 micron. The Poynting vector describes the flux of energy and is related to the absorbance per unit volume per unit per unit time, Q, by

$$\text{div } \mathbf{S} + \frac{\mathrm{d}Q}{\mathrm{d}t} = 0. \tag{7}$$

The log of the magnitude of the Poynting vector and its direction along the first 300 nm of a 1 μm device are shown in Fig. 5 for the two excitation wavelengths. It is desired to simplify the structure and emphasize the physical explanation of the observed phenomena. Therefore, we have simulated a 1 μm device in order to reduce the interference between the propagating and reflected wave along the z axis.

Figure 5 shows that there is a flow of energy from the

Downloaded 05 May 2010 to 132.72.54.88. Redistribution subject to AIP license or copyright; see http://jap.aip.org/jap/copyright.jsp

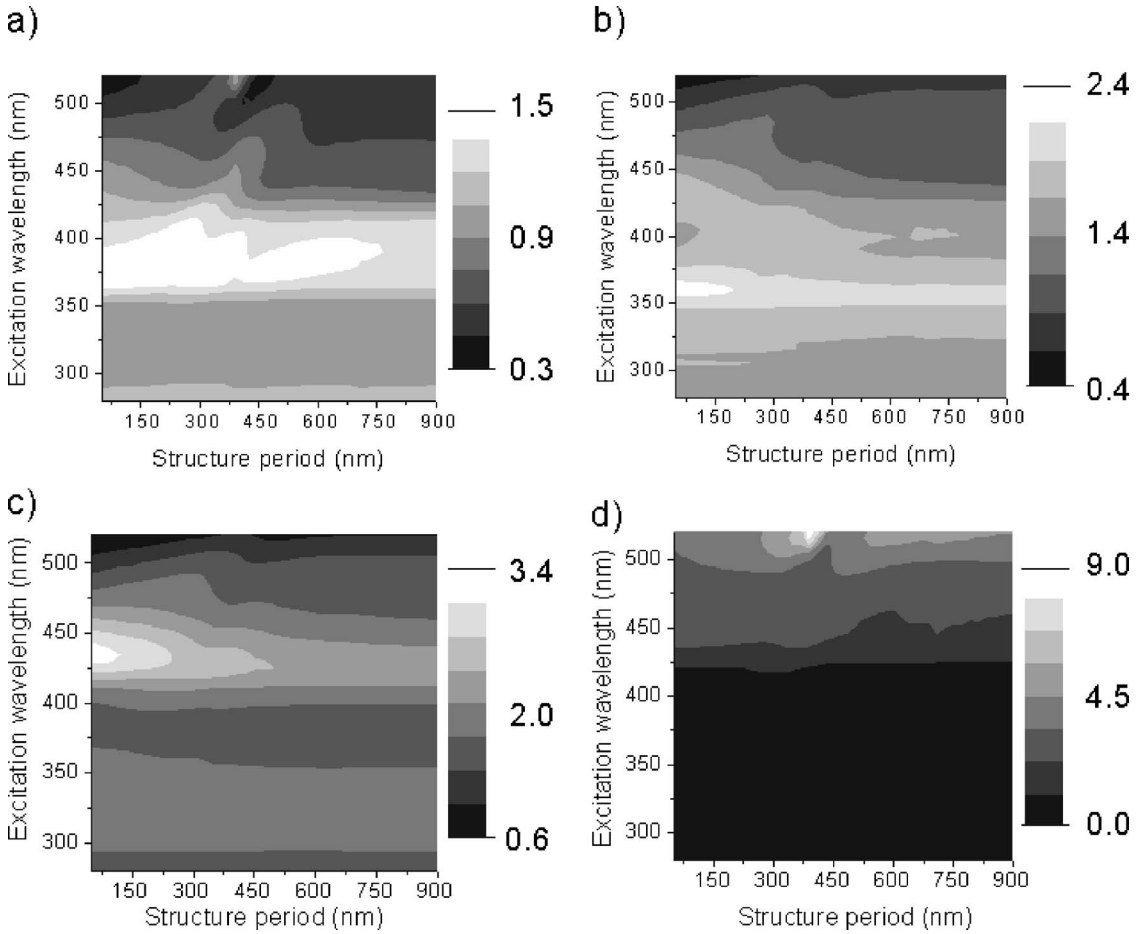

FIG. 4. The dependence of the ratio between the absorption in a lateral periodic structure and a bilayer structure, $\hat{I}$, on the structure period, $2d$, and on the excitation wavelength for film thicknesses of 50 nm and different device structures. Structures without a mirror with "FP" (a) and "PF" (b) configuration. Structures with a mirror with "FP" (c) and "PF" (d) configuration. Enhanced absorption is indicated by brighter colors, with values of $\hat{I}$ as indicated by the bars.

material with the lower absorption coefficient to the material with the higher absorption coefficient where it is absorbed. This process cannot happen in the a framework where scattering is not present.

The behavior of the absorption in the last region, the region in which there is a linear dependence of the excitation wavelength on the structure period, can be explained by investigating the propagation of the wave front along the interface between the two homopolymers. When a plane wave incidents normal to the material surface, an electrical field component E_z is produced at the boundary between the two homopolymers to satisfy the boundary condition.[22] This component of the electric field does not propagate but rather resonates in a direction perpendicular to the propagating direction. This resonance occurs in the periodical direction and is therefore sensitive to the length of the period, $2d$. When the excitation wavelength is equal to the period length or is half its size, constructive interference occurs and the amplitude of E_z is large. This results in enhancement of the absorption as seen is Fig. 3. The magnitude of E_z^2 for the cases

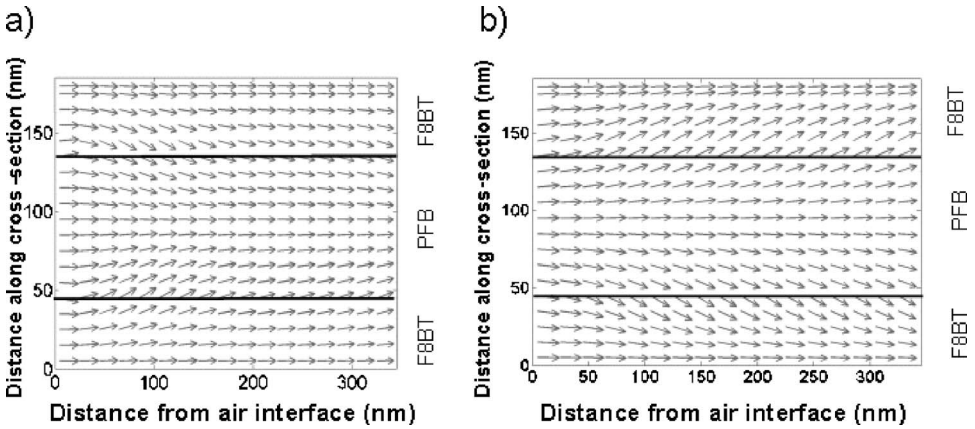

FIG. 5. The log of the magnitude of the Poynting vector and its direction along the first 300 nm of the devices. Excitation wavelength 360 (a) and 440 nm (b).

Downloaded 05 May 2010 to 132.72.54.88. Redistribution subject to AIP license or copyright; see http://jap.aip.org/jap/copyright.jsp

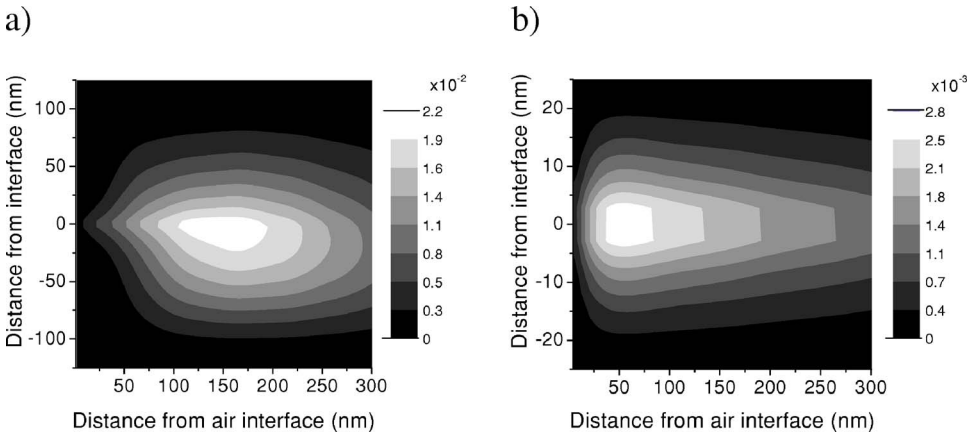

FIG. 6. The amplitude of E_z^2 at the vicinity of the PFB/F8BT interface (PFB at the top and F8BT at the bottom) for excitation wavelength of 500 nm. In resonance $2d=500$ nm (a) and out of resonance, $2d=100$ nm (b).

of in and out of resonance is shown in Fig. 6 for structures with periods of 100 and 500 nm, and for the first 300 nm of a 1 μm thick device under excitation wavelength of 500 nm.

Figure 6 shows the square of the amplitude of the electromagnetic field component E_z along the interface between PFB and F8BT for two different structure periods in and out of resonance. Figure 6(a) shows a structure with a period of 500 nm while in Fig. 6(b) the structure period is 100 nm. It can be seen that the maximum of the electric field in resonance [Fig. 6(a)]is an order of magnitude larger than the field out of resonance [Fig. 6(b)]. In addition, the spreading of the peak is four times larger. Therefore, an enhanced absorption is expected in the 500 nm period structure compared to the 100 nm period structure. This is indeed observed in Fig. 3.

The above reasoning explains the behavior of the absorption for structures that do not have mirrors at their ends [Figs. 2(a), 3(a), 3(c), and 3(e)]. The presence of the mirror complicates the picture because there is an interference between waves that propagate in the positive and negative direction of the z axis. However, we can see that in general the behavior remains the same as in the structure without the mirror. The maximum enhancement in the absorbance is still around 470 nm and the two lobes corresponding to the resonance of E_z are still present. However, these lobes are wider than in the no-mirror case and they can even overlap. In most of the structures we see that the absorption ratio increases with the presence of a mirror.

Our reasoning can also explain the results depicted in Fig. 4 using the above arguments. In Figs. 4(a) and 4(b) we see enhancement in the absorption around 450 and 330 nm. In both regions the absorption of the PFB is much smaller than the F8BT and therefore, the energy transfer from the PFB into the F8BT that is induced by scattering at the interfaces in the periodical structure enhances the absorption. These two subfigures also show the appearance of enhancement lobes in the region where there is low absorption in both materials. This is due to constructive interference, as explained above, which is only present in the periodical structure.

In Figs. 4(c) and 4(d) the picture is much more complicated because of the presence of the mirror at the end of the device. The effect of diffraction is large enough to dominate the entire spectrum as seen in Fig. 4(d). We can see in Figs. 4(a)–4(c) the presence or the beginning of lobes. The most important observation is that a 50 nm periodical structure with period below 400 nm can outperform, in the sense of absorption, the two bilayer configurations of the same thickness. This indicates that the energy transfer in the periodical structure is very efficient.

IV. CONCLUSION

In this article we have compared numerical and no-scattering analytical calculations of the expected absorption of photocells fabricated from conjugated polyfluorene polymers. We have also compared two different configurations for photocells, bilayer and periodical structures.

The absorption was calculated for a periodical structure with a period $2d$ whose period was perpendicular to the propagation of the light. We have shown the importance of scattering in this structure by showing that the numerically calculated absorbance can be 2.6 times larger than the one calculated analytically by neglecting scattering. We have also compared structures with mirrors at their ends to those that do not have mirrors and saw similar behavior. The absorption was enhanced, i.e., scattering is important, in particular in two different regions. The first wavelength region is where only one of the polymers absorbs and the other has minimum absorbance. In this area the periodical material behaves like a leaky waveguide with the energy leaking from the less absorbent material to the more absorbent one. The second region is where both materials have low or no absorbance. In this region it is the resonance behavior of the scattered electric field which dominates the absorption. When the excitation wavelength is equal to or double the structure period, constructive interference results in enhanced absorbance. When comparing the bilayer configurations to the periodical configuration, we have found that the periodical structure outperforms the bilayer configuration.

The significance of this work is therefore not only in the indication of the importance of scattering, but also as a design tool. Our approach enables the tuning of the device specifications in accordance with the constituent materials and the light profile to achieve optimal absorbance.

An optimal absorbance does not necessarily mean optimal efficiency because there are additional physical processes that contribute to the efficiency such as charge generation, charge conduction, and charge collection whose

Downloaded 05 May 2010 to 132.72.54.88. Redistribution subject to AIP license or copyright; see http://jap.aip.org/jap/copyright.jsp

dependence on the structure can be different. However, it is reasonable to assume that higher absorbance will lead to higher efficiency. Moreover, calculating the absorption profile gives vital information that is currently missing.

The above approach can be extended to three-dimensional structures, to more than two polymers, and to blend structures and complex geometries.

ACKNOWLEDGMENTS

This work was supported by the EU Integrated Project NAIMO (No NMP4-CT-2004-500355)

[1]C. W. Tang, Appl. Phys. Lett. **48**, 183 (1986).
[2]C. Brabec, N. Sariciftci, and J. Hummelen, Adv. Funct. Mater. **11**, 15 (2001).
[3]M. Granström, K. Petritsch, A. C. Arias, A. Lux, M. R. Andersson, and R. H. Friend, Nature **395**, 257 (1998).
[4]S. E. Shaheen, D. S. Ginley, and H. E. Jabbour, MRS Bull. **30**, 10 (2005).
[5]W. Ma, C. Yang, X. Gong, K. Lee, and A. J. Heeger, Adv. Funct. Mater. **15**, 1617 (2005).
[6]J. M. Halls, A. C. Arias, J. D. Mackenzie, W. Wu, M. Inbasekaran, E. P. Woo, and R. H. Friend, Adv. Mater. **12**, 498 (2000).
[7]E. Moons, J. Phys.: Condens. Matter **14**, 12235 (2002).
[8]G. A. Buxton and N. Clarke, Phys. Rev. B **74**, 085207 (2006).
[9]H. Hoppe, N. Arnold, N. S. Sariciftci, and D. Meissner, Sol. Energy Mater. Sol. Cells **80**, 105 (2003).
[10]B. Harbecke, Appl. Phys. B **39**, 165 (1986).
[11]O. S. Heavens, *Optical Properties of Thin Solid Films* (Dover, New York, 1991).
[12]P. K. Watkins, A. B. Walker, and G. L. B. Verschoor, Nano Lett. **5**, 1814 (2005).
[13]K. Yee, IEEE Trans. Antennas Propag. **14**, 302 (1966).
[14]A. Taflove and S. C. Hagness, *Computational Electrodynamics: The Finite-Difference Time-Domain Method*, 3rd ed. (Artech House, London, 2005).
[15]M. Redecker, D. Bradley, M. Inbasekaran, W. Wu, and E. Woo, Adv. Mater. **11**, 241 (1999).
[16]C. M. Ramsdale and N. C. Greenham, J. Phys. D **36**, L29 (2003).
[17]R. Shikler, M. Chiesa, and R. H. Friend, Macromolecules **39**, 5393 (2006).
[18]J. P. Berenger, J. Comput. Phys. **127**, 363 (1996).
[19]D. E. Merewether, R. Fisher, and F. W. Smith, IEEE Trans. Nucl. Sci. **27**, 1829 (1980).
[20]G. Mur, IEEE Trans. Electromagn. Compat. **EMC-23**, 377 (1981).
[21]K. R. Umashankar and A. Taflove, IEEE Trans. Electromagn. Compat. **EMC-24**, 397 (1982).
[22]H. Sato, H. Domae, and M. Takahashi, Trans. Inst. Electr. Eng. Jpn., Part B **J82**-B, 674 (1999).

Downloaded 05 May 2010 to 132.72.54.88. Redistribution subject to AIP license or copyright; see http://jap.aip.org/jap/copyright.jsp